This is the accepted version of the following article: Fu HR, Cao YT, Qu Z. Substructural shake table testing for nonstructural elements of various damage sensitivity in a fixed-base and a base-isolated building. ***Earthquake Engineering & Structural Dynamics***. This article may be used for non-commercial purposes.

A full-scale shake table test on the torsional responses of base-isolated structures by friction pendulums

Haoran Fu[1,2], Yuteng Cao[2,3], Zhe Qu[1,2*]

1. Key Laboratory of Earthquake Engineering and Engineering Vibration, Institute of Engineering Mechanics, China Earthquake Administration, No.1 Chaobai Street, Yanjiao, Sanhe, Hebei 065201, China.

2. Key Laboratory of Earthquake Disaster Mitigation, Ministry of Emergency Management, Harbin 150080, China.

3. College of Civil Engineering, Xi'an University of Architecture and Technology, Xi'an, China.

Abstract: Torsional response remains an important concern in the seismic performance of base-isolated structures. In this study, a full-scale shake table test was conducted on a three-layer FPB-isolated structure, together with numerical simulations and bearing component tests, to investigate its torsional behavior and three potential sources of torsion: superstructure flexibility, pressure dependence of the friction coefficient, and bearing-to-bearing variability in the friction coefficient. The results show that, compared with the transient eccentricity (ε_k), the proposed effective transient eccentricity (ε_s) provides a clearer indication of torsional response because it directly represents the effective lever arm producing torsion. Superstructure flexibility increases ε_s by altering the instantaneous distribution of inertia forces, although the resulting torsional displacement amplification remains limited. The torsional response observed in the shake table tests is mainly associated with variability in the friction coefficient, whereas the pressure dependence of the friction coefficient has a relatively limited influence. These findings provide a mechanical interpretation of the torsional response of FPB-isolated structures and highlight the importance of considering variability in individual bearing properties in torsional assessment.

Keywords: eccentricity, overturning moment, superstructure flexibility, friction coefficient, pressure dependence

1 Introduction

Numerous earthquakes have demonstrated that structures are highly vulnerable to severe torsional damage during earthquakes. For instance, the 1972 Managua earthquake, the 1985 Mexico City earthquake, and the 1999 Izmit and Duzce earthquakes caused extensive structural damage and even collapse in many buildings due to torsional irregularities (Brown, 1973; Bertero, 1980; Chandler, 1986; Hall, 1986; Meli, 1986; Gokdemir, 2013).

Seismic isolation is supposed to mitigate both translational and torsional responses of structures by lengthening the fundamental period and enhancing energy dissipation (Lee, 1980). Nevertheless, numerical studies by Nagarajaiah et al. (1993) on a three-story rubber bearing–isolated frame showed that torsional effects may still be amplified when the center of mass (CM) does not coincide with the center of stiffness (CS) in the isolation layer. Jangid and Datta (1994a, 1994b) confirmed this through nonlinear analysis of a single-story rubber isolated frame structure, further emphasizing that isolation layer eccentricity significantly affects the maximum displacement of the isolation bearings. Subsequent

Correspondence: Zhe Qu, Email: quz@iem.ac.cn

This is the accepted version of the following article: Fu HR, Cao YT, Qu Z. Substructural shake table testing for nonstructural elements of various damage sensitivity in a fixed-base and a base-isolated building. ***Earthquake Engineering & Structural Dynamics***. This article may be used for non-commercial purposes.

studies examined this issue from different perspectives. Wolff et al. (2014) emphasized the influence of the ratio between effective translational and torsional periods on displacement amplification. Mazza (2017) investigated the lateral-torsional response of buildings isolated with curved surface sliding systems under near-fault ground motions, including the effects of friction-related parameters. Laguardia et al. (2019) proposed a simplified method for predicting torsional effects in asymmetric seismically isolated buildings subjected to bidirectional earthquake components. Cavdar and Ozdemir (2022) further examined the amplification of maximum isolator displacement in LRB-isolated buildings due to mass eccentricity. These studies demonstrate that torsional response remains an important consideration in the seismic design of base-isolated structures.

In contrast to rubber bearings, friction pendulum bearings (FPB) exhibit a distinct torsional mechanism. Since both the pendulum restoring force and the frictional force of an FPB are proportional to its axial load (Zayas, 1990), the effective horizontal stiffness of the bearings is also proportional to the axial load. Consequently, under gravity loads alone, the CS of the FPB-isolated layer always coincides with the CM with zero actual eccentricity. Zayas (1990) argued that this characteristic makes FPB particularly effective in mitigating torsional effects within the isolation layer.

Previous studies have argued that, although FPBs possess the aforementioned characteristics, torsion in FPB-isolated structures may still arise from various sources (de la Llera and Almazán, 2003; Almazán and de la Llera, 2003). Torsion induced by known mass and stiffness eccentricities of the superstructure is referred to as actual torsion, whereas torsion resulting from uncertainties in frictional behavior, manufacturing tolerances of bearings, accidental eccentricities in mass and stiffness, torsional components of ground motion, or overturning moments of the superstructure is termed accidental torsion.

To investigate these effects, De la Llera and Almazan (2003) conducted a series of shake table tests on FPB-isolated structures. In tests on an isolation layer consisting of four FPBs and a slab without a superstructure, they attributed torsion mainly to the velocity dependence of the friction coefficient and initial variations in the friction coefficient. However, two concerns arise from this interpretation. First, when torsion does not occur or its amplitude is small, the velocities of all bearings remain nearly identical, indicating no causal link between torsion and the velocity dependence of the friction coefficient. Second, in their analysis, the authors merely increased or decreased the friction coefficients of bearings along two orthogonal directions by 5% and assessed plausibility based on simulation results, which appears overly arbitrary. Based on this work, they further tested a three-story FPB-isolated structure on a shake table and concluded that additional torsion originated from the variation in axial force induced by overturning moments, which shifted the position of the CS and thus generated torsional effects.

Similarly, Becker et al. (2012) concluded that overturning moments were the primary source of torsion in FPB-isolated layers, which they assessed by interpreting the offset between the CS and CM in terms of its two orthogonal components. However, both De la Llera and Becker neglected the influence of the direction of base shear force relative to the CS. Simply considering the CS shift is insufficient to explain the causes of torsion.

Moreover, the experiments conducted by Becker et al. (2012) exhibited several unexplained phenomena. For instance, when the upper mass blocks were placed in an eccentric configuration, the torsional amplitudes observed were considerably larger than those predicted numerically, even though the isolation layer itself had no actual eccentricity. In addition, in some symmetric mass configurations, torsional responses of the isolation layer even exceeded those under eccentric mass arrangements. These anomalies suggest that torsional behavior is more likely attributable to significant discrepancies in the friction coefficients of FPBs, an issue not addressed in their study.

This is the accepted version of the following article: Fu HR, Cao YT, Qu Z. Substructural shake table testing for nonstructural elements of various damage sensitivity in a fixed-base and a base-isolated building. ***Earthquake Engineering & Structural Dynamics***. This article may be used for non-commercial purposes.

This study investigates three potential sources of torsion through full-scale shake table testing and numerical simulations: superstructure flexibility, pressure dependence of the friction coefficient, and variability in the friction coefficient.

2 Analytical torsional responses of FPB-isolated structures

Fig. 1(a) illustrates a minimum planar model of an FPB-isolated structure subjected to gravity only. The weight associated with the i-th level is denoted as W_i, and the total weight of the superstructure is $W=\Sigma W_i$. The distances from the left- and right-hand side friction pendulum bearings to the CM are represented by l_1 and l_2, respectively. P_1 and P_2 denote the vertical forces acting on the two bearings, the equilibrium of moments of which guarantees $P_1/P_2 = l_2/l_1$. On the other hand, the equivalent lateral stiffness k_{eq} of each FPB is calculated by Eq. (1) (Mokha et al., 1996):

$$k_{\mathrm{eq}} = \frac{P}{R} + \mu\frac{P}{\delta}\mathrm{sgn}(\dot{\delta}) = P\left[\frac{1}{R} + \frac{\mu}{\delta}\mathrm{sgn}(\dot{\delta})\right] \tag{1}$$

where R is the equivalent radius of the FPB, μ is the friction coefficient of the FPB, and $\mathrm{sgn}(\cdot)$ is the sign function.

When there is no torsion in the isolation layer, all bearings within the isolation layer exhibit the same displacement (δ) and velocity direction ($\dot{\delta}$), and therefore the equivalent lateral stiffness k_{eq} of each bearing is directly proportional to its axial load P, i.e., $k_{\mathrm{eq}} \propto P$. It leads to $P_1/P_2 = k_{\mathrm{eq1}}/k_{\mathrm{eq2}} = l_2/l_1$, suggesting that the CS in the out-of-plane direction of the system coincides with the CM. In other words, the initial eccentric distance in the FPB-isolated system, denoted as e_0, is zero. This is consistent with the conclusion of Zayas et al. (1990).

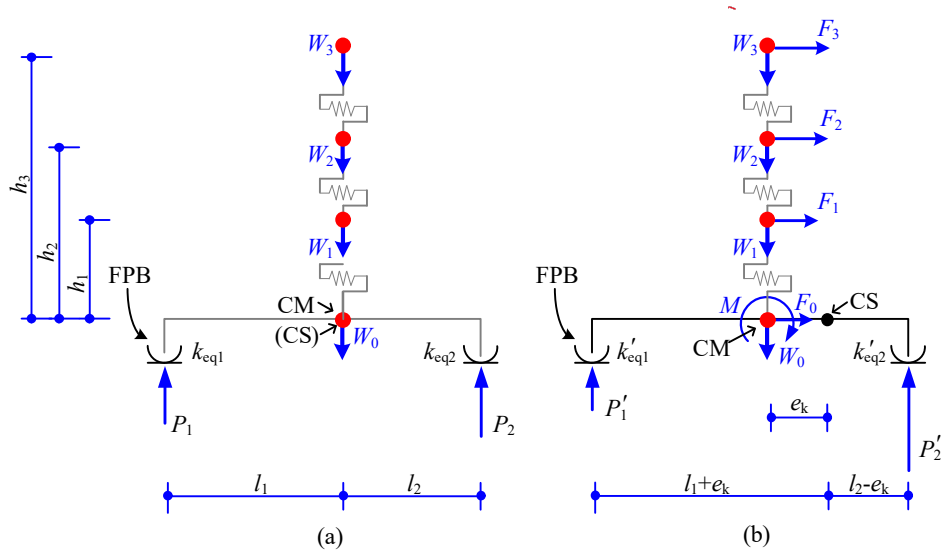

Fig. 1. Force state of FPB under (a) gravity only, and (b) combined gravity and seismic excitation.

When the structure is subjected to horizontal seismic excitation, the horizontal inertia force acting at the i-th level is denoted as F_i [Fig. 1(b)]. The resultant horizontal force and overturning moment are $F=\Sigma F_i$ and $M=\Sigma F_i h_i$, respectively, where h_i is the height of the i-th level above the isolation layer. In this case, the vertical forces P_1' and P_2' acting on the two bearings are:

$$P_1' = \frac{l_2 W - M}{l_1 + l_2}, \quad P_2' = \frac{l_1 W + M}{l_1 + l_2} \tag{2}$$

Correspondingly, the equivalent lateral stiffnesses k'_{eq1} and k'_{eq2} of the two FPBs will change but

This is the accepted version of the following article: Fu HR, Cao YT, Qu Z. Substructural shake table testing for nonstructural elements of various damage sensitivity in a fixed-base and a base-isolated building. ***Earthquake Engineering & Structural Dynamics***. This article may be used for non-commercial purposes.

remain proportional to their axial forces, i.e.:

$$\frac{k'_{\mathrm{eq1}}}{k'_{\mathrm{eq2}}} = \frac{P'_1}{P'_2} = \frac{l_2 W - M}{l_1 W + M} = \frac{l_2 - M/W}{l_1 + M/W} \tag{3}$$

It is clear that the CS and the CM no longer coincide. The transient eccentric distance, denoted e_{k}, is:

$$e_{\mathrm{k}} = \frac{M}{W} \tag{4}$$

It is the parameter used by Becker et al. (2012) to evaluate torsional response, which is independent of the mass eccentricity of the superstructure. When the resultant shear force in the isolation layer is sufficiently large, the contribution of the decomposed friction term to the directional force relationship becomes relatively small. Therefore, to derive a simplified analytical expression for the subsequent discussion, the friction term is neglected in the following derivation. The above results are valid only for the planar isolation system under unidirectional out-of-plane horizontal seismic motion. In realistic cases, the structure is always subjected to bidirectional seismic motion as illustrated in Fig. 2(a), where F_{xi} and F_{yi} represent the horizontal seismic forces acting on the i-th floor in the x and y directions, respectively. M_x and M_y are the corresponding overturning moments, while V_x and V_y denote the base shear forces in the x and y directions. Given the same W of the superstructure, the orthogonal components of the transient eccentric distances e_{k} in the orthogonal directions are proportional to the respective overturning moments, i.e.:

$$\frac{e_{\mathrm{kx}}}{e_{\mathrm{ky}}} = \frac{M_x}{M_y} = \frac{\sum_{i=1}^{U}(F_{xi}h_i)}{\sum_{i=1}^{U}(F_{yi}h_i)} \tag{5}$$

where e_{kx} and e_{ky} are the components of e_{k} in the x and y directions, respectively. Here, i is the floor number, and U denotes the total number of floors. As long as the lateral force distributions in both orthogonal directions are the same, that is, $F_{x1}:F_{x2}:\cdots:F_{xU} = F_{y1}:F_{y2}:\cdots:F_{yU}$, as is the case for a rigid superstructure, the orthogonal components e_{kx} and e_{ky} will be proportional to the base shear V in the same directions. Therefore, the resultant base shear force V always passes through the CS, and no torque will result from the transient eccentricity e_{k} [Fig. 2(b)].

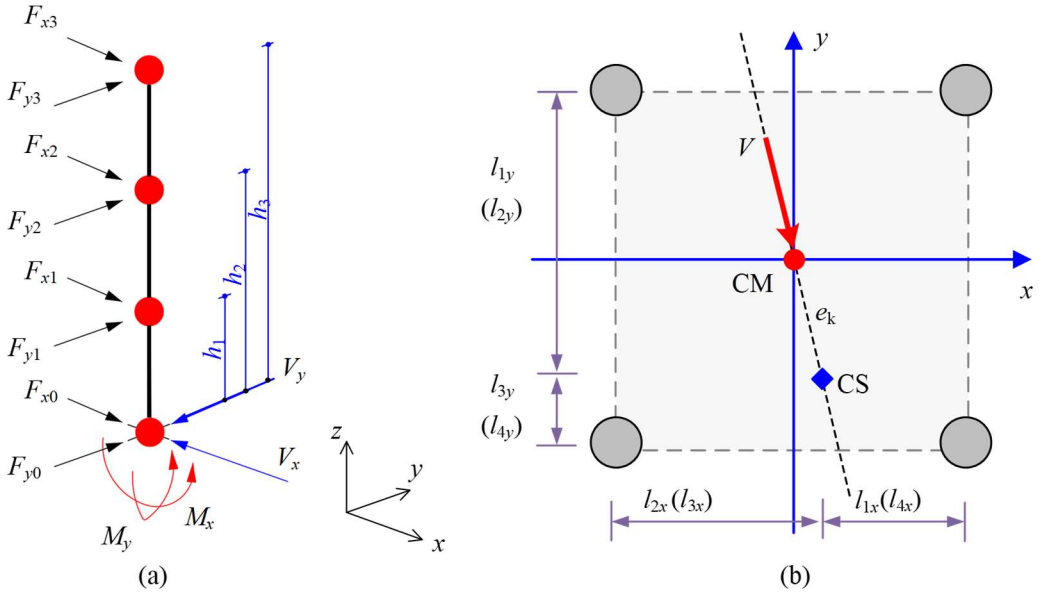

This is the accepted version of the following article: Fu HR, Cao YT, Qu Z. Substructural shake table testing for nonstructural elements of various damage sensitivity in a fixed-base and a base-isolated building. ***Earthquake Engineering & Structural Dynamics***. This article may be used for non-commercial purposes.

Fig. 2. FPB-isolated system with rigid superstructure: (a) forces on the superstructure, and (b) base shear and the transient CS in the FPB isolation layer.

When the superstructure is flexible as shown in Fig. 3(a), however, inter-story deformation alters the instantaneous inertia force distributions along the height under bidirectional excitation. Consequently, the condition of $F_{x1}:F_{x2}:\cdots:F_{xU}=F_{y1}:F_{y2}:\cdots:F_{yU}$ does not always hold. As a result, the base shear V may not always pass through the transient CS, producing a nonzero torsional moment, as illustrated in Fig. 3(b). In this case, the torsional moment is governed by the distance from the transient CS of the isolation layer to the base shear V vector. This distance is referred to as the effective transient eccentric distance, and is denoted as e_s, hereinafter.

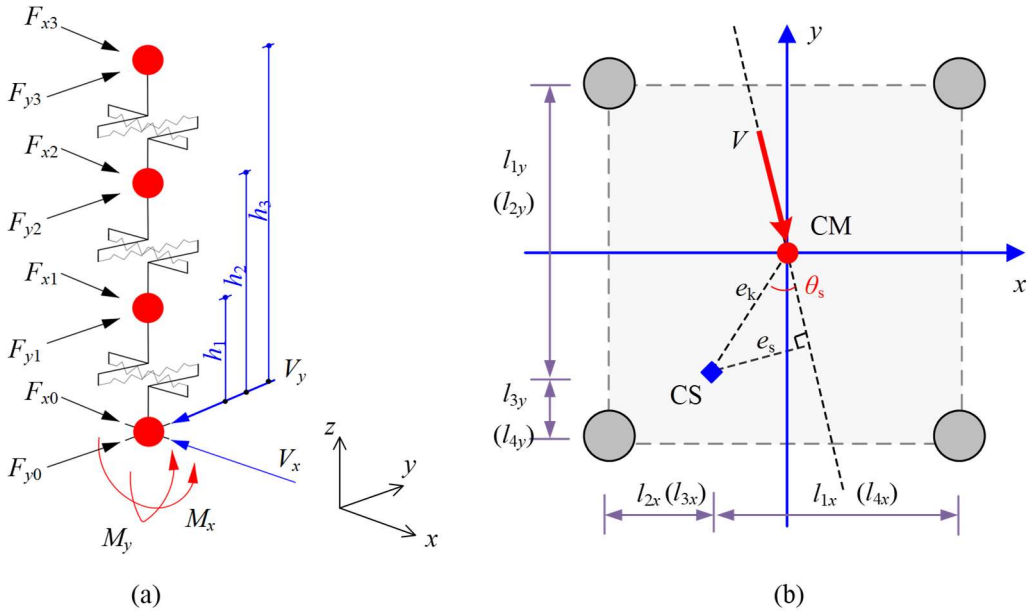

Fig. 3. FPB-isolated system with flexible superstructure: (a) forces on the superstructure, and (b) base shear and the transient CS in the FPB isolation layer.

Following the common practice of defining eccentricities in the seismic design of buildings (e.g., JGJ 99-2015(2015)), the above eccentric distances, e_0, e_k and e_s are normalized by their respective torsional radii to yield the actual eccentricities (ε_0), transient eccentricities (ε_k) and effective transient eccentricities (ε_s) [Eq. (6)], respectively.

$$\varepsilon_0=\frac{e_0}{\gamma_{e0}}\cdot\mathrm{sgn}(e_{ky}),\qquad \varepsilon_k=\frac{e_k}{\gamma_{es}}\cdot\mathrm{sgn}(e_{ky}),\qquad \varepsilon_s=\frac{e_s}{\gamma_{es}}\cdot\mathrm{sgn}(\theta_s) \tag{6}$$

where γ_{es} is the transient torsional radius calculated from the instantaneous lateral stiffness of the isolation bearings.

$$\gamma_{es}=\sqrt{\frac{K_T}{\sum_{n=1}^{N}k_n}} \tag{7}$$

$$K_T=\sum_{n=1}^{N}(k_n l_{nx}^2)+\sum_{n=1}^{N}(k_n l_{ny}^2) \tag{8}$$

where N is the total number of bearings, k_n is the instantaneous tangent stiffness of the n-th bearing, K_T is the total torsional stiffness of the isolation layer. l_{nx} and l_{ny} are the instantaneous distances from the n-th bearing to the CS in the x and y directions, respectively. Accordingly, γ_{es} varies during motion, and

This is the accepted version of the following article: Fu HR, Cao YT, Qu Z. Substructural shake table testing for nonstructural elements of various damage sensitivity in a fixed-base and a base-isolated building. ***Earthquake Engineering & Structural Dynamics***. This article may be used for non-commercial purposes.

γ_{e0} is the initial value of γ_{es}. The functions $\mathrm{sgn}(e_{ky})$ and $\mathrm{sgn}(\theta_s)$ are sign functions. If the CS is located above the *x*-axis, $\mathrm{sgn}(y_k)$ takes the value of 1; if it is located below the *x*-axis, $\mathrm{sgn}(y_k)$ takes the value of -1. Similarly, if the CS is positioned in the clockwise direction of *V*, $\mathrm{sgn}(\theta_s)$ takes the value of 1; if it is in the counterclockwise direction, $\mathrm{sgn}(\theta_s)$ takes the value of -1.

ε_k and ε_s are both dynamic quantities associated with the migration of the CS during seismic excitation. ε_k characterizes the instantaneous offset between the CM and the transient CS, and therefore reflects the migration of the CS caused by the redistribution of axial forces. However, a nonzero ε_k does not necessarily produce torsion, because the torsional moment also depends on the positional relationship between the resultant base shear *V* and the transient CS. In contrast, ε_s is defined by the perpendicular distance from the transient CS to the line of action of *V*, and therefore directly represents the effective lever arm producing torsion. Consequently, ε_s may remain small even when ε_k is nonzero if *V* passes through or close to the transient CS.

3 Shake table test and numerical simulation

3.1 Test setup

A full-scale shake table test was conducted to verify the efficacy of ε_0, ε_k, and ε_s on the torsion of FPB-isolated structures. The specimen was a three-layer FPB-isolated steel structure (Fig. 4), referred to as NEST (Nonstructural Element Simulator on Shake Table) in Fu et al. (2024) and Cao et al. (2024).

The stiffness of the steel parts of the three layers is sufficiently large to ensure it behaves like a rigid body during the vibration, while the lateral flexibility of the system was mainly provided by the FPBs, natural rubber bearings (NRB), and springs in between the steel parts. The stiffness of the isolation layer, denoted as k_A, is attributed to four full-scale FPBs with an equivalent radius of curvature of 1.6 m and a total stroke of 1200mm. The stiffnesses of the two stories of the superstructure were represented by k_B and k_C, respectively, where k_B is governed by four NRBs and k_C by four small FPBs in parallel with 16 tension springs.

Shear keys between the steel parts can be optionally installed to provide additional lateral stiffnesses of 9174 kN/mm for k_B and 2709 kN/mm for k_C, respectively (Fig. 4c). They are much larger than those of the bearings and springs so that the lateral flexibility of the superstructure is effectively eliminated. By installing or removing the shear keys, the test specimen can be switched between a rigid-superstructure system (RS) and a flexible-superstructure system (FS), thereby allowing for the investigation of the influence of superstructure flexibility on the torsional response. In addition, to examine the effect of actual eccentricity in the superstructure, 240 kg of mass blocks on the 1st and 3rd floors were rearranged from one side to the other to generate an actual eccentric distance of 166mm in the superstructure (Fig. 4d), corresponding to an ε_0 of 3.33% under the assumption that the CS remains fixed. This was done for the rigid-superstructure system and is denoted as an RS-E case.

The stiffness and mass of each story are listed in Table 1. Based on the design, the RS, RS-E, and FS systems share an identical isolation layer and exhibit similar mass distributions along the height. The fundamental periods of these systems, calculated based on the tangent stiffness, together with the corresponding test-identified periods, are summarized in Table 2, while the first-mode shapes are shown in Fig. 5. For the FS system, the effective modal mass ratio for the first-mode shape reaches 99.3%, indicating that the structural response is predominated by the first mode, although a small contribution from higher-order modes is present in the FS system.

This is the accepted version of the following article: Fu HR, Cao YT, Qu Z. Substructural shake table testing for nonstructural elements of various damage sensitivity in a fixed-base and a base-isolated building. ***Earthquake Engineering & Structural Dynamics***. This article may be used for non-commercial purposes.

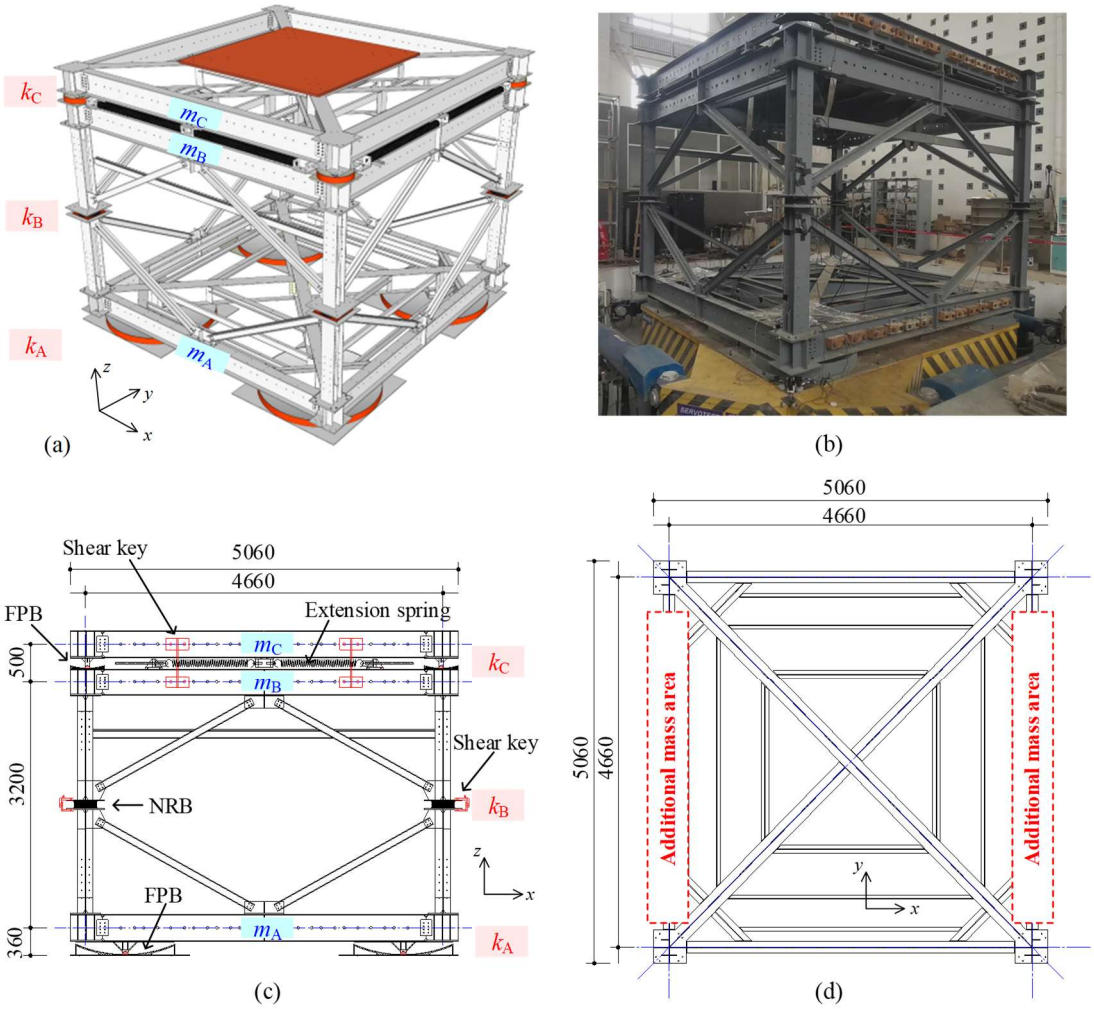

Fig. 4. Overview of the NEST: (a) 3D model, (b) photograph of the full-scale test specimen, (c) front view, and (d) plan layout.

Table 1. Parameter design in different systems

	Mass (kg)				Tangent stiffness (N/mm)		
System	m_A	m_B	m_C	Total	k_A	k_B	k_C
RS	4194	4408	4862	13464	82.07	-	-
RS-E	3714+m_e	4408	4282+m_e	13464	82.07	-	-
FS	4194	4287	4609	13090	79.79	2000	192.13

Note: m_e=480kg is the mass of the eccentric installation.

Table 2. Periods of different systems

Mode	RS		RS-E		FS		Direction
	Calculated	Identified	Calculated	Identified	Calculated	Identified	
1	2.55s	2.47s	2.57s	2.52s	2.64s	2.57s	*x*
2	2.55s	2.43s	2.55s	2.42s	2.64s	2.52s	*y*
3	2.18s	—	2.16s	—	2.25s	—	Torsion

This is the accepted version of the following article: Fu HR, Cao YT, Qu Z. Substructural shake table testing for nonstructural elements of various damage sensitivity in a fixed-base and a base-isolated building. ***Earthquake Engineering & Structural Dynamics***. This article may be used for non-commercial purposes.

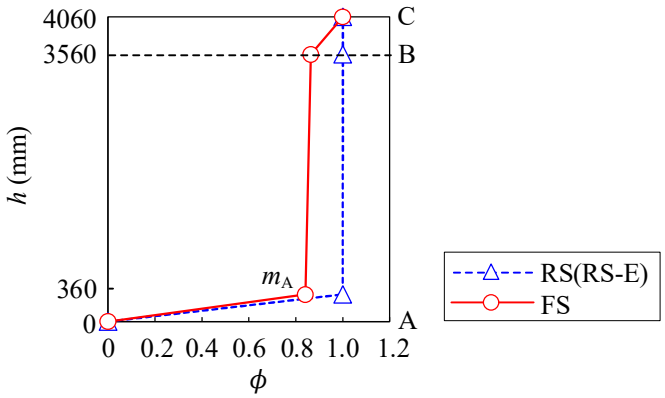

Fig. 5. First-mode shape of RS, RS-E and FS systems.

3.2 Component testing of friction coefficients

The coefficient of friction (μ) of the bearings is a critical parameter affecting the torsional response of the structure, and μ was calibrated through component tests before performing the shake table test. Since the full-scale FPB bearings at the isolation layer of NEST were too large for the available testing facility, only the smaller FPBs between the top two layers of NEST were tested. Both types of FPB bearings were provided by the same manufacturer, using identical materials and surface treatments, and their frictional properties can be regarded as statistically equivalent.

The small FPBs were tested on the multi-axis loading facility at the Institute of Engineering Mechanics (IEM). The specimen was connected to a triaxial load cell in series and anchored to the base girder of the facility at the bottom. The top of the load cell was fixed to the loading platen, which was driven by four horizontal and four vertical hydraulic actuators to provide displacement-controlled loading in both the vertical and horizontal directions. A pair of wire transducers was installed to measure the displacement at the top and bottom of the specimen. More details of the test setup can be found in Fu et al. (2024).

Eight small FPBs, including the four used in the test, were subjected to three cycles of sinusoidal horizontal displacement history of ±6mm amplitude and 0.0025Hz frequency, as per the GB/T 37358-2019 (2019). To capture the possible effect of normal pressure on μ (Tsopelas et al., 1996; Constantinou et al., 1999), the horizontal loading of each bearing was repeated when it was under a constant vertical compression force of 18.1kN and 11.3kN. They correspond to vertical pressures of 7.9MPa and 4.9MPa on the sliding surface, respectively, matching the vertical pressures experienced by the full-scale FPBs and small FPBs under gravity-only conditions. Fig. 6(a) depicts the hysteresis curves of the horizontal-to-vertical force ratio and lateral displacement in the third cycle of loading. The coefficient of friction is taken as the horizontal-to-vertical force ratio at zero lateral displacement, which is determined by the linear regression of the hysteresis curve segments within ±3mm lateral displacement. As summarized in Fig. 6(b), the mean friction coefficient ($\bar{\mu}_A$) was 2.4% and the standard deviation (σ_A) was 0.32% at 7.9MPa. At a lower pressure of 4.9 MPa, the mean friction coefficient ($\bar{\mu}_C$) was 2.9%, and the standard deviation (σ_C) was 0.47%. As shown in Fig. 6(b), the decay of μ with increased pressure can be well represented by Eq. (9) (Constantinou et al., 1999).

$$\mu(P) = k\frac{P}{A_0}^{\eta-1} \tag{9}$$

where k and η are the parameters, A_0 is the contact area of the slider, and P is the axial force on the FPB.

This is the accepted version of the following article: Fu HR, Cao YT, Qu Z. Substructural shake table testing for nonstructural elements of various damage sensitivity in a fixed-base and a base-isolated building. ***Earthquake Engineering & Structural Dynamics***. This article may be used for non-commercial purposes.

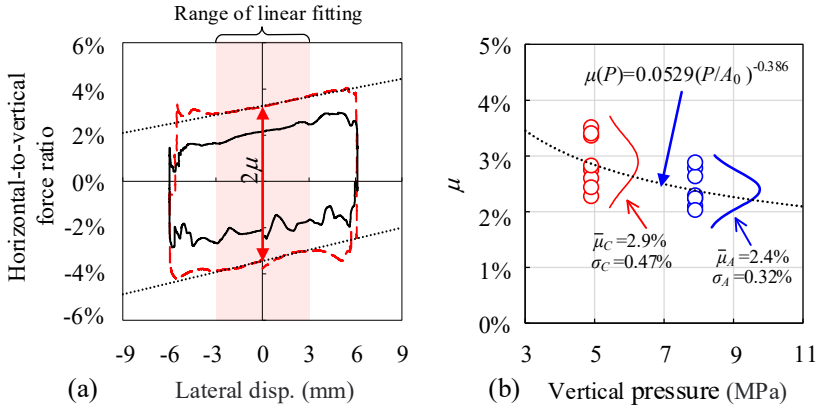

Fig. 6. Friction coefficient test: (a) extraction of friction coefficients and (b) test results and empirical fitting.

3.3 Ground motions and instrumentation

The RS, RS-E, and FS systems are assumed to be subjected to the three bi-directional strong earthquake shakings listed in Table 3, with their time-histories illustrated in Fig. 7(a). To accommodate the stroke of the available shake table, all ground motion records were processed using a high-pass filter with a cutoff frequency of 0.2 Hz.

The acceleration response spectra (S_a) of the selected ground motion records are compared with the design response spectrum for Seismic Intensity 8 in the Chinese seismic code (GB/T 50011-2010, 2010) in Fig. 7(b). Among the ground motion records, MZQ exhibits the highest spectral acceleration at the fundamental period, with one component exceeding the design response spectrum. In contrast, TAF has the smallest spectral value at the fundamental period, with both components reaching only 31%~42% of the design response spectrum.

The bidirectional horizontal components of the three ground motion records were scaled by the peak acceleration in the x-direction before being used as the shake table motion. The target peak table accelerations in the x-direction (PTA_x) for the different cases are shown in Fig. 7(c). The numerical simulations of the NEST model were conducted using the measured shake table responses as input ground motions.

Table 3. Ground motion records for shake table tests

ID	Event	Station	Component	*PGA* (g)	Loading direction
EL	Imperial Valley, 1940	El-Centro	EL-NS	0.349	*x*
			EL-EW	0.214	*y*
TAF	Kern County, 1952	Taft Lincoln School	TAF-111	0.180	*x*
			TAF-021	0.159	*y*
MZQ	Wenchuan, 2008	MZQ	MZQ-EW	0.954	*x*
			MZQ-NS	0.844	*y*

This is the accepted version of the following article: Fu HR, Cao YT, Qu Z. Substructural shake table testing for nonstructural elements of various damage sensitivity in a fixed-base and a base-isolated building. ***Earthquake Engineering & Structural Dynamics***. This article may be used for non-commercial purposes.

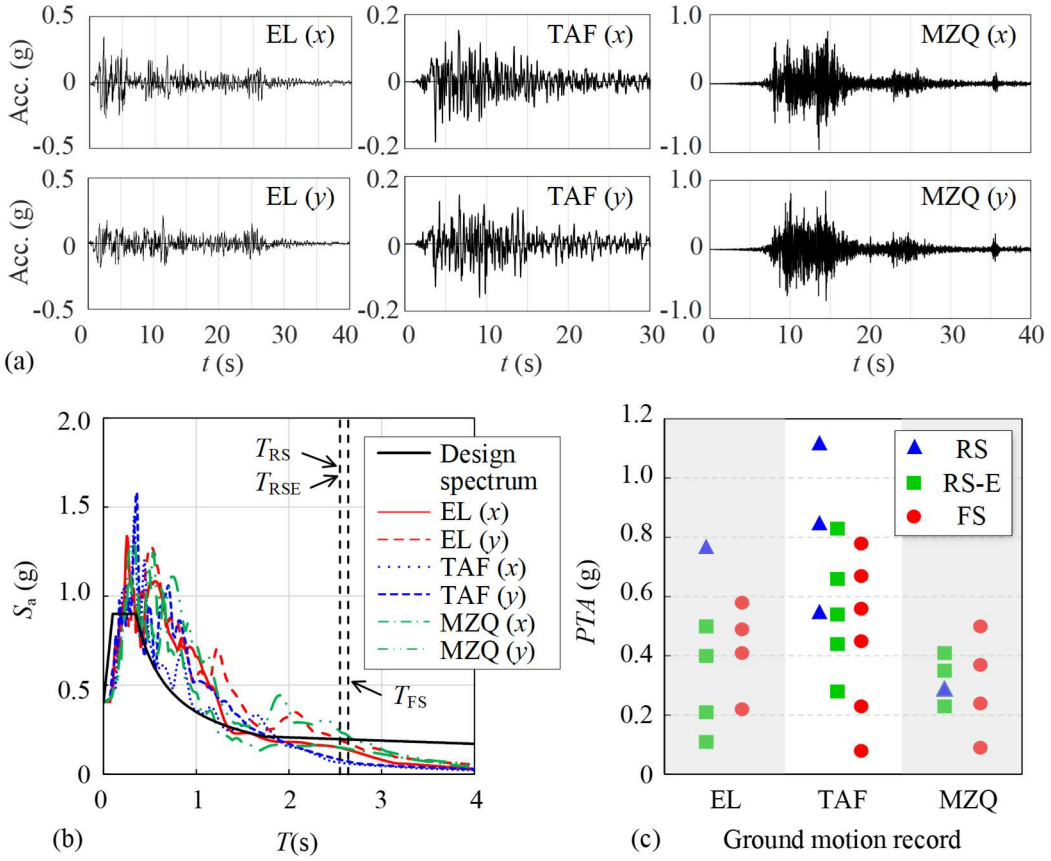

Fig. 7. Selected ground motion records: (a) acceleration time histories, (b) acceleration response spectra at 5% damping, and (c) load cases of shake table test.

Two accelerometers, a_{T1} and a_{T2}, were mounted on the shake table to monitor the table motion. Four displacement transducers (i.e., u_{Ai}, u_{Bi}, and u_{Ci}, i=1 to 4) were arranged between each layer of the testbed and a scaffold for instrumentation to measure the torsion of each layer. Additional displacement transducers, u_{FPB}s, were arranged between the shake table and the bottom layer of the testbed to measure the displacement of the isolation layer (Fig. 8). The translational displacement of the isolation layer in the orthogonal directions (u_x, u_y) can be calculated by Eq. (10) and Eq. (11). The torsion (θ) of the isolation layer can be calculated by Eq. (12).

$$u_x = (u_{\mathrm{FPB1}} - u_{\mathrm{FPB2}})/2 \tag{10}$$

$$u_y = (u_{\mathrm{FPB3}} + u_{\mathrm{FPB4}})/2 \tag{11}$$

$$\theta = \arcsin\left(\frac{u_{\mathrm{Ay1}} - u_{\mathrm{Ay2}} + u_{\mathrm{Ax1}} - u_{\mathrm{Ax2}}}{2L_{\mathrm{FPB}}}\right) \tag{12}$$

where L_{FPB} is the horizontal distance between the two displacement transducers used for calculating the rotation angle.

In previous studies, the ratio of the maximum displacement at an edge of the isolation layer to the displacement of the geometric center at the same instant has been used as an indicator of torsional displacement amplification (de la Llera and Almazan, 2003; Almazan and de la Llera, 2003; Olivares, 2020). In the present study, λ can be calculated from the torsional and translational responses of the isolation layer according to Eq. (13).

This is the accepted version of the following article: Fu HR, Cao YT, Qu Z. Substructural shake table testing for nonstructural elements of various damage sensitivity in a fixed-base and a base-isolated building. ***Earthquake Engineering & Structural Dynamics***. This article may be used for non-commercial purposes.

$$\lambda_x = \frac{2\max\{|u_{Ax1}(t_x^*)|, |u_{Ax2}(t_x^*)|\}}{|u_{Ax1}(t_x^*) + u_{Ay2}(t_x^*)|} \qquad \lambda_y = \frac{2\max\{|u_{Ay1}(t_y^*)|, |u_{Ay2}(t_y^*)|\}}{|u_{Ay1}(t_y^*) + u_{Ay2}(t_y^*)|} \tag{13}$$

where t_x^* and t_y^* denote the instants corresponding to the maximum absolute displacements among u_{Ax1}, u_{Ax2} and u_{Ay1}, u_{Ay2}, respectively.

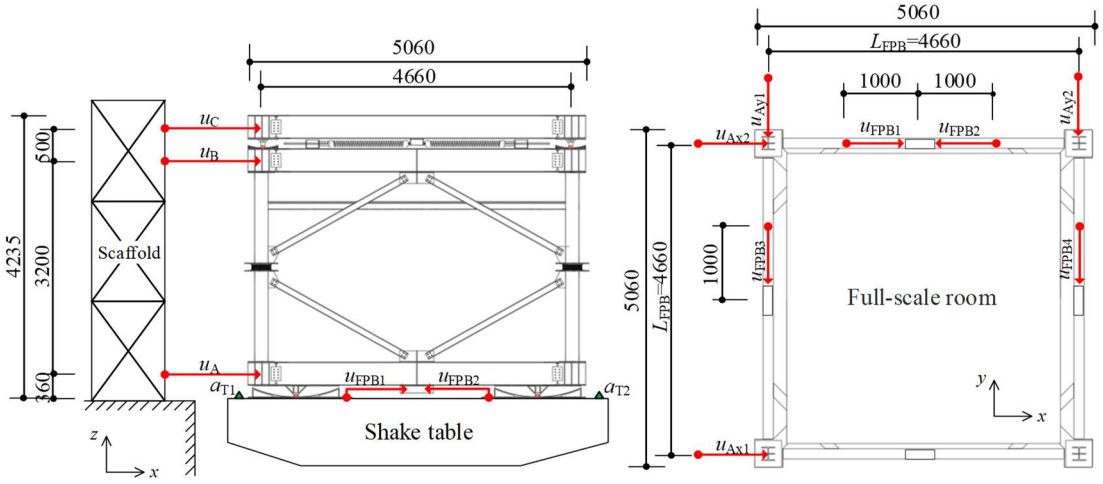

Fig. 8. Instrument arrangement (unit: mm)

3.4 Numerical model

A member-by-member finite element model of the NEST was built in OpenSees (McKenna, 2011) to assist in the analysis of the torsional behavior of NEST. The FPBs were modeled using the *singleFPBearing* element, while the NRBs and springs were modeled by the *twoNodeLink* element with *uniaxialMaterial Elastic* material (Fig. 9). For simulating the RS and RS-E systems, the stiffnesses of the bearings at the second and third stories were set to the corresponding stiffnesses of the shear keys specified in Section 3.1 to effectively constrain structural deformation. The steel frame, being sufficiently strong to remain within the elastic regime without yielding or buckling, was modeled using *elasticBeamColumn* elements for its braces, beams, and columns. The uniform masses of the *elasticBeamColumn* elements per unit length were calculated based on the cross-sections, additional mass, and other components. In this numerical model, Coulomb friction is used, with the friction coefficient of the full-scale FPBs taken as $\bar{\mu}_A$, and the friction coefficient of the small FPBs is assigned based on experimental results.

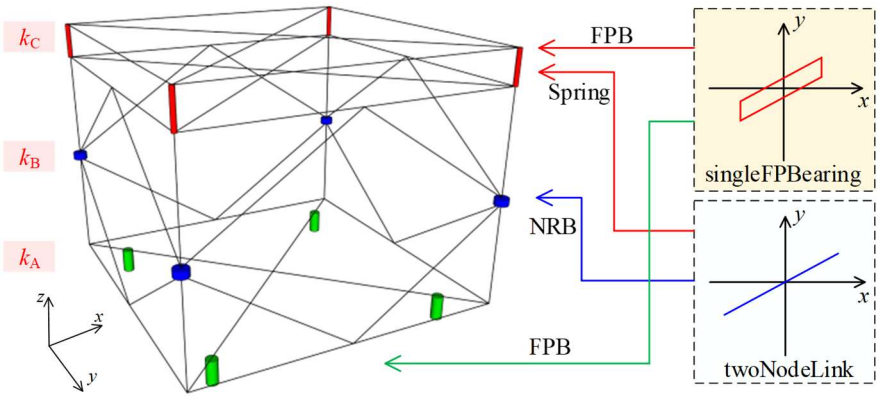

Fig. 9. Numerical model of the NEST.

This is the accepted version of the following article: Fu HR, Cao YT, Qu Z. Substructural shake table testing for nonstructural elements of various damage sensitivity in a fixed-base and a base-isolated building. ***Earthquake Engineering & Structural Dynamics***. This article may be used for non-commercial purposes.

4 Experimental and simulated responses

The time-history responses of the isolation layer obtained from the experiments and numerical simulations for the RS, RS-E, and FS systems under the maximum *PTA* condition are shown in Fig. 10, Fig. 11, and Fig. 12, respectively. The comparison indicates that the numerical model accurately simulates the translational response, with relative errors of the peak responses (ϵ) between the simulation and the test ranging from 0.5% to 14.7%. However, the torsional response is underpredicted, with relative errors reaching 99.7%.

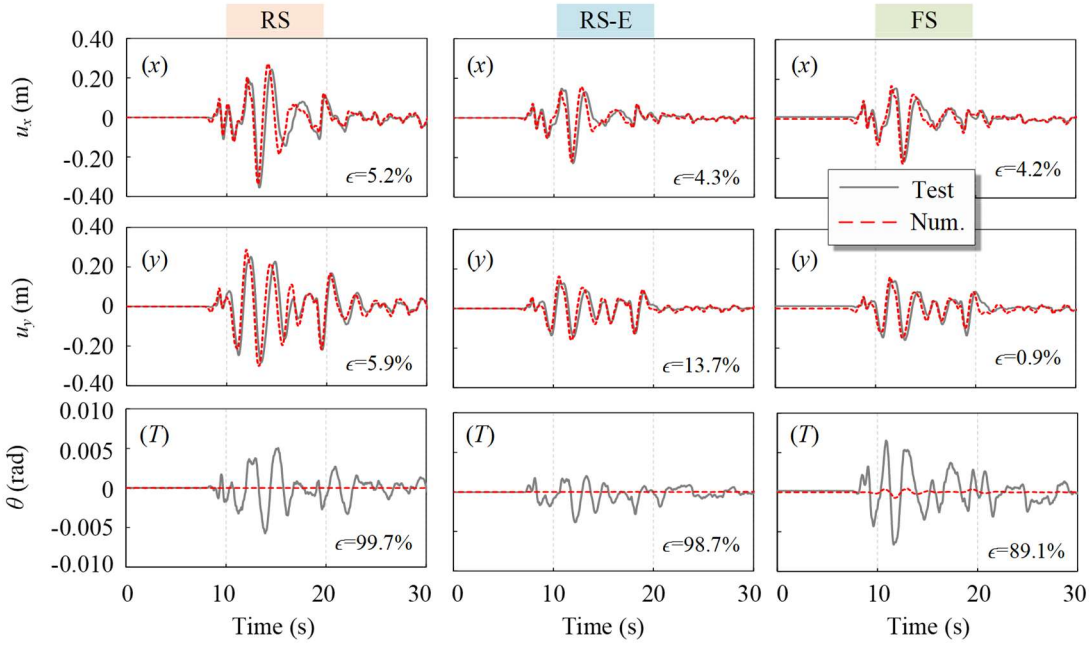

Fig. 10. Comparison of numerical and experimental results under EL excitation.

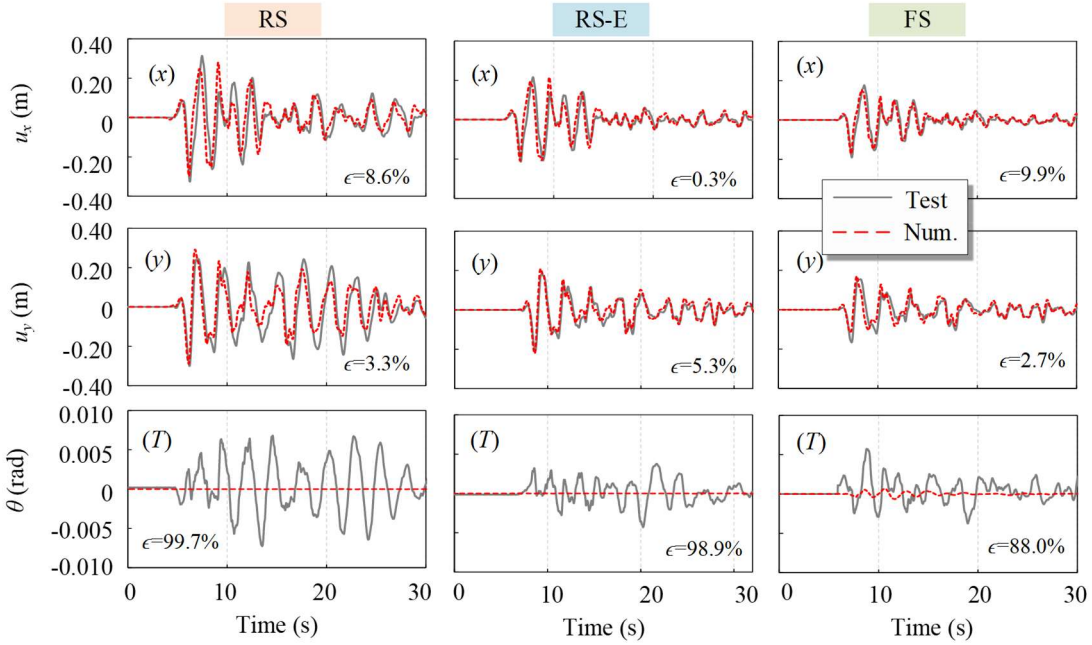

Fig. 11. Comparison of numerical and experimental results under TAF excitation.

This is the accepted version of the following article: Fu HR, Cao YT, Qu Z. Substructural shake table testing for nonstructural elements of various damage sensitivity in a fixed-base and a base-isolated building. ***Earthquake Engineering & Structural Dynamics***. This article may be used for non-commercial purposes.

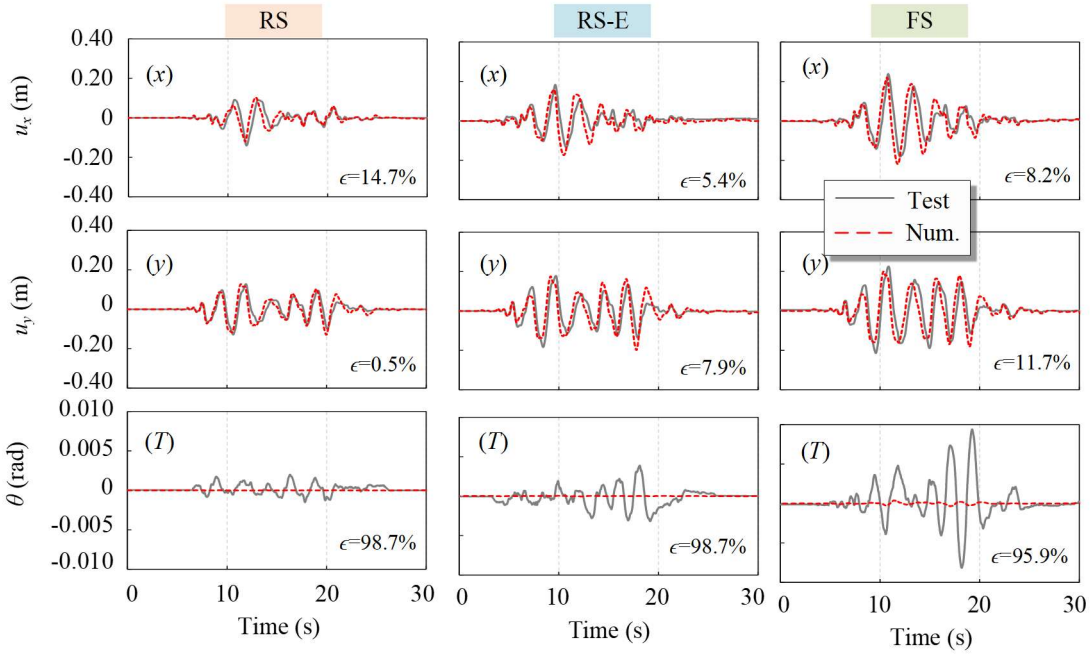

Fig. 12. Comparison of numerical and experimental results under MZQ excitation.

The numerical results clearly show that the FS system develops an evident torsional response, whereas the torsional responses of the RS and RS-E systems remain negligible. This observation is consistent with the theoretical discussion in Section 2, which indicates that superstructure flexibility promotes the development of a nonzero effective transient eccentricity and consequently increases the torsional tendency of the isolation layer. In the shake table tests, however, appreciable additional torsional responses are observed, including in the RS and RS-E systems, which are not reproduced by the idealized numerical model. This residual discrepancy is attributed primarily to the bearing-to-bearing variability of the friction coefficients, which is not represented in the model used for Figs. 10-12. The causes of this additional torsional response are further analyzed and discussed in Section 5.2.

The results of λ under the maximum *PTA* conditions are summarized in Table 4.

Table 4. Values of λ under the maximum *PTA* conditions

	x-direction			*y*-direction		
	RS	RS-E	FS	RS	RS-E	FS
EL	1.017	1.018	1.031	1.002	1.041	1.041
TAF	1.005	1.005	1.002	1.008	1.022	1.001
MZQ	1.011	1.005	1.010	1.007	1.004	1.006

As shown in Table 4, the values of λ remain small for all three systems, including the FS system. This is because λ is governed by the displacement state at the instant when the maximum edge displacement occurs, while the torsional rotation does not necessarily reach its peak at the same instant. Therefore, even when noticeable torsional response develops during the response history, its contribution to the maximum edge displacement may remain limited. Taking the torsional displacement-ratio criterion of 1.20 specified in GB/T 50011-2010 (2010) as a reference, all calculated λ values are below this limit, with a maximum value of 1.041. This indicates that the torsional response observed in the present tests does not result in significant amplification of the maximum edge displacement.

To further compare the response-based λ with the conventional period-based measure used in

This is the accepted version of the following article: Fu HR, Cao YT, Qu Z. Substructural shake table testing for nonstructural elements of various damage sensitivity in a fixed-base and a base-isolated building. ***Earthquake Engineering & Structural Dynamics***. This article may be used for non-commercial purposes.

seismic isolation design, the torsional displacement amplification factor λ_{ASCE} was evaluated using the ASCE formulation (Eq. (14)).

$$\lambda_{\mathrm{ASCE}} = \frac{D_{\mathrm{TM}}}{D_{\mathrm{M}}} = 1 + \left(\frac{y}{P_{\mathrm{T}}^2}\right)\frac{12e}{b^2 + d^2} \tag{14}$$

where D_{M} and D_{TM} are the maximum displacements at the center of rigidity and at the element of interest, respectively; y is the distance from the center of rigidity to the element of interest; b and d are the plan dimensions; e is the eccentricity; and P_{T} is the ratio of the effective translational period to the effective torsional period of the isolation system.

For this conventional calculation, the center of rigidity of the isolation system was assumed to remain fixed at the geometric center, and the axial-load-dependent migration of the FPB center of stiffness toward the center of mass was intentionally disregarded. This assumption was applied only in evaluating λ_{ASCE} and was not introduced into the calculation of ε_{s} or the nonlinear numerical model. If the load-dependent migration of the FPB center of stiffness were retained, the imposed mass eccentricity in the RS-E system would not produce a persistent offset between the center of mass and the center of stiffness; consequently, its contribution to λ_{ASCE} would remain unity when accidental eccentricity is excluded.

Based on the geometric configuration of the test structure and the calculated periods reported in Table 2, the 5% accidental eccentricity results in a λ_{ASCE} of approximately 1.10 for the RS and FS systems. For the RS-E system, the imposed mass eccentricity of 166mm is combined with the 5% accidental eccentricity, resulting in a governing λ_{ASCE} of approximately 1.17. These code-based estimates exceed the maximum response-based amplification ratio of 1.04 reported in Table 4, indicating that the ASCE expression provides a conservative estimate of edge-displacement amplification for the FPB systems.

The comparison also highlights the different physical meanings of λ_{ASCE} and ε_{s}. λ_{ASCE} is a design-oriented measure determined by the prescribed eccentricity and the translational-to-torsional period ratio under the assumption of a fixed center of stiffness. This assumption is more consistent with conventional rubber-bearing isolation systems than with FPB systems, because their lateral stiffness is not directly governed by the instantaneous axial load in the same manner as that of FPBs. In contrast, ε_{s} is a transient, mechanism-based parameter that accounts for both the migration of the FPB center of stiffness and the instantaneous line of action of the resultant base shear. Therefore, ε_{s} is more suitable for interpreting the torsional mechanism of FPB-isolated structures, whereas λ_{ASCE} remains useful as a conventional design-oriented estimate of torsional displacement amplification.

5 Sources of torsional responses

5.1 Superstructure flexibility

Based on the numerical model and the Coulomb friction, ε_{s}, ε_{k} and torsional angle of the isolation layer under idealized conditions can be calculated in detail.

To facilitate a quantitative comparison, Figs. 13-15 present θ, ε_{k}, and ε_{s} of the isolation layer under different ground motion excitations at a *PTA* of 0.4g. The results indicate that the ε_{s} values of the RS and RS-E systems are nearly identical and remain very small. Under the MZQ excitation, the maximum ε_{s} for the RS and RS-E systems are 2.05% and 2.24%, respectively. This suggests that the base shear V in the RS and RS-E systems consistently remains very close to the CS of the isolation layer. Correspondingly, the isolation layers in these systems exhibit negligible torsion, consistent with the conclusions drawn in Section 2.

This is the accepted version of the following article: Fu HR, Cao YT, Qu Z. Substructural shake table testing for nonstructural elements of various damage sensitivity in a fixed-base and a base-isolated building. ***Earthquake Engineering & Structural Dynamics***. This article may be used for non-commercial purposes.

The value of ε_s for the FS system becomes larger throughout the time domain, with a maximum value of 4.45% under EL excitation. This indicates a noticeable deviation between the direction of V and the position of the CS, accompanied by torsional behavior in the isolation layer. The maximum torsional angle observed in the FS system reaches 0.00031rad, even when ε_0 is zero. In contrast, irrespective of whether torsion occurs in the isolation system, the results of ε_k are consistently similar in all systems, with the maximum values significantly large. This further substantiates that ε_k tends to overestimate the torsional behavior of FPB structures.

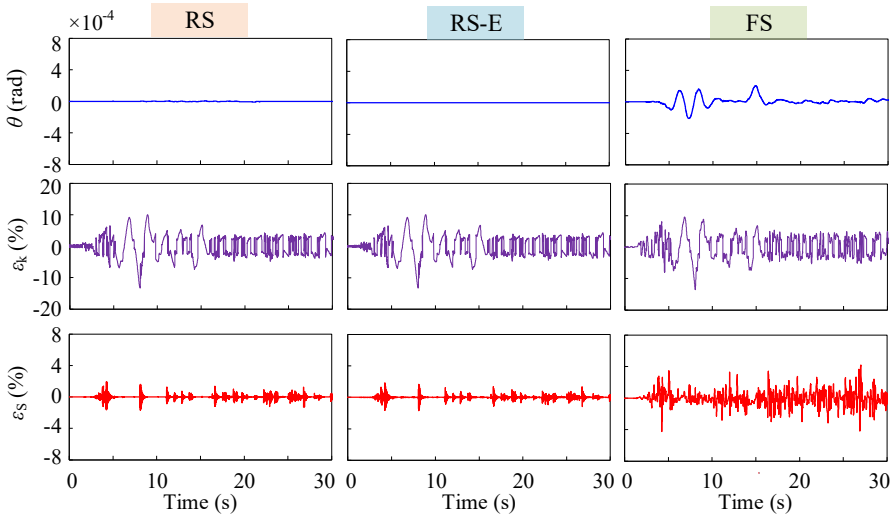

Fig. 13. Torsion response and eccentricity of the FPB isolation layer under EL excitation.

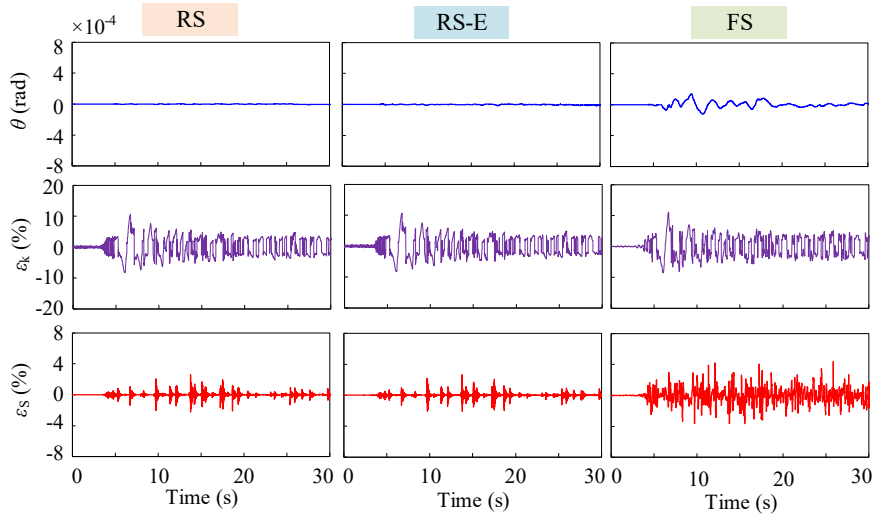

Fig. 14. Torsion response and eccentricity of the FPB isolation layer under TAF excitation.

This is the accepted version of the following article: Fu HR, Cao YT, Qu Z. Substructural shake table testing for nonstructural elements of various damage sensitivity in a fixed-base and a base-isolated building. ***Earthquake Engineering & Structural Dynamics***. This article may be used for non-commercial purposes.

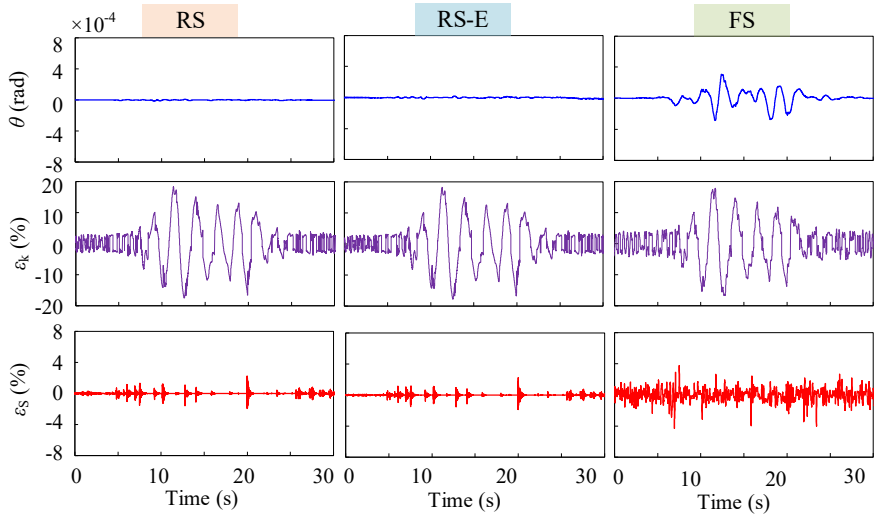

Fig. 15. Torsion response and eccentricity of the FPB isolation layer under MZQ excitation.

In all simulation conditions corresponding to the tests, Fig. 16 compares the relationships of $\varepsilon_{s,max}$ and $\varepsilon_{k,max}$ with the maximum torsional angle (θ_{max}). As shown in Figs. 16(a) and 16(b), $\varepsilon_{s,max}$ exhibits a clearer correspondence with θ_{max} than $\varepsilon_{k,max}$. This improved correspondence between ε_s and θ_{max} further supports the rationality of the proposed effective transient eccentricity.

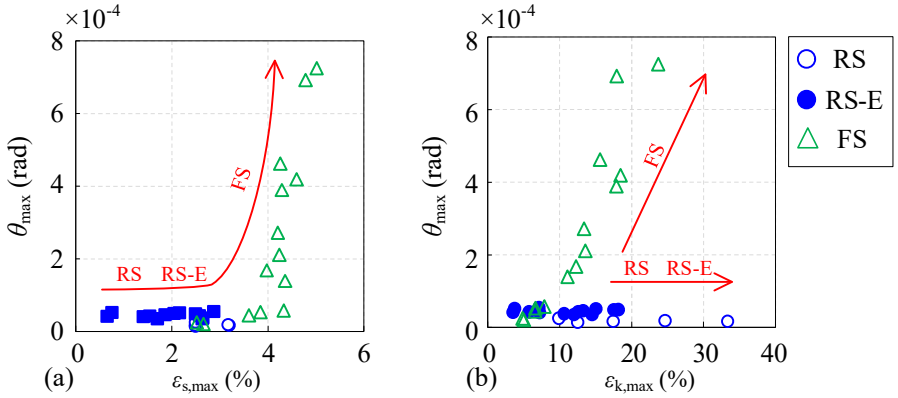

Fig. 16. The correlation between θ_{max} and (a) ε_s and (b) ε_k.

From an engineering perspective, ε_s can be used as a mechanism-based post-processing indicator in bidirectional nonlinear response-history analysis. It can be evaluated at each time step from the transient CS and the instantaneous line of action of the resultant base shear V, and the joint histories of ε_s and V can be used to identify response instants with elevated torsional potential. The corresponding edge displacement, torsional rotation, and individual bearing deformation can then be examined at these critical instants. At present, ε_s is intended to supplement rather than replace conventional response-based design checks, and no general acceptance threshold is proposed based on the limited structural and loading conditions investigated in this study.

5.2 Variation of friction coefficients

Although the numerical model reasonably reproduces the translational responses and the relative torsional tendencies of the three structural configurations, it does not fully capture the magnitude of the measured torsional response, suggesting the presence of an additional source of torsion that is not represented in the idealized model. To quantitatively assess this discrepancy, the relationship between the maximum torsional angle (θ_{max}) and the maximum translational displacement (u_{max}) of the isolation

This is the accepted version of the following article: Fu HR, Cao YT, Qu Z. Substructural shake table testing for nonstructural elements of various damage sensitivity in a fixed-base and a base-isolated building. ***Earthquake Engineering & Structural Dynamics***. This article may be used for non-commercial purposes.

layer is examined. Here, u_{max} and θ_{max} are independently extracted from their respective time-history responses and therefore do not necessarily occur at the same instant. The experimental and numerical results for the RS and RS-E systems are presented in Fig. 17, while those for the FS system are shown in Fig. 18. The results show that, under all loading cases, the experimentally measured θ_{max} values are substantially larger than the corresponding numerical predictions.

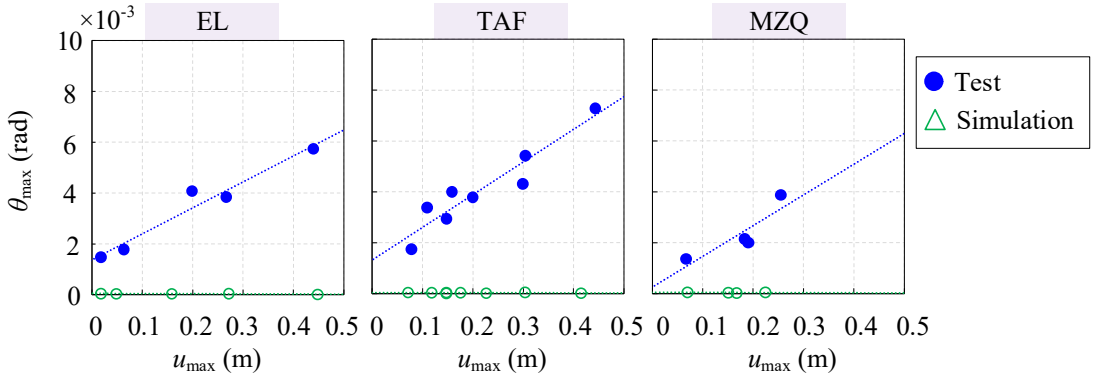

Fig. 17. Comparison of experimental and simulated results for the RS and RS-E systems.

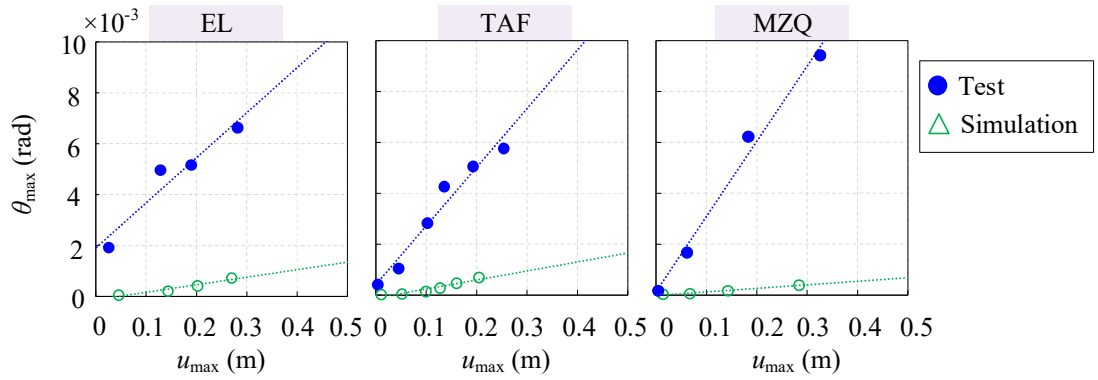

Fig. 18. Comparison of experimental and simulated results for the FS system.

The component tests in Section 3.2 show that the friction coefficient varies with the axial pressure of the bearings. To investigate whether the torsional response is caused by overturning-moment-induced variations in axial pressure and the resulting changes in the friction coefficient, the constant friction coefficient in the numerical model was replaced by a pressure-dependent friction coefficient, $\mu(P)$. The parameters of $\mu(P)$ were calibrated based on the component-test results in Section 3.2. The resulting maximum torsional responses were then compared with those obtained using a constant friction coefficient, as shown in Fig. 19.

This is the accepted version of the following article: Fu HR, Cao YT, Qu Z. Substructural shake table testing for nonstructural elements of various damage sensitivity in a fixed-base and a base-isolated building. ***Earthquake Engineering & Structural Dynamics***. This article may be used for non-commercial purposes.

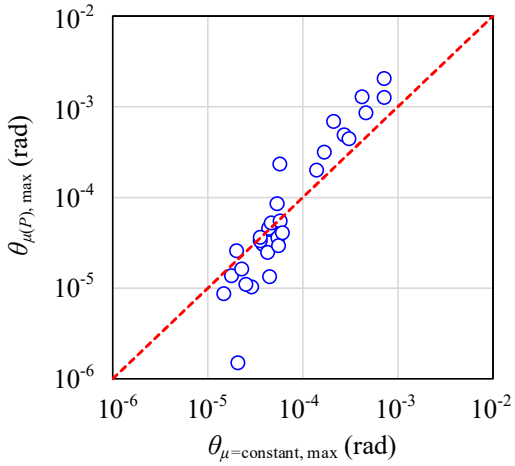

Fig. 19. Effect of the pressure-dependent friction coefficient on θ_{max}.

The results indicate that the pressure dependence of the friction coefficient has some influence on the torsional response; however, its effect is far too small to account for the discrepancy between the experimental and numerical results shown in Figs. 17 and 18. Taking the response under EL excitation at a *PTA* of 0.75g as an example, the variation in bearing axial pressure induced by the overturning moment causes the friction coefficient to reach a maximum of 4.92% (Fig. 20(a)). However, the friction force accounts for only approximately 9.6% of the total horizontal force at this condition (Fig. 20(b)). Therefore, the pressure dependence of the friction coefficient has only a limited influence on the torsional response of the isolation layer.

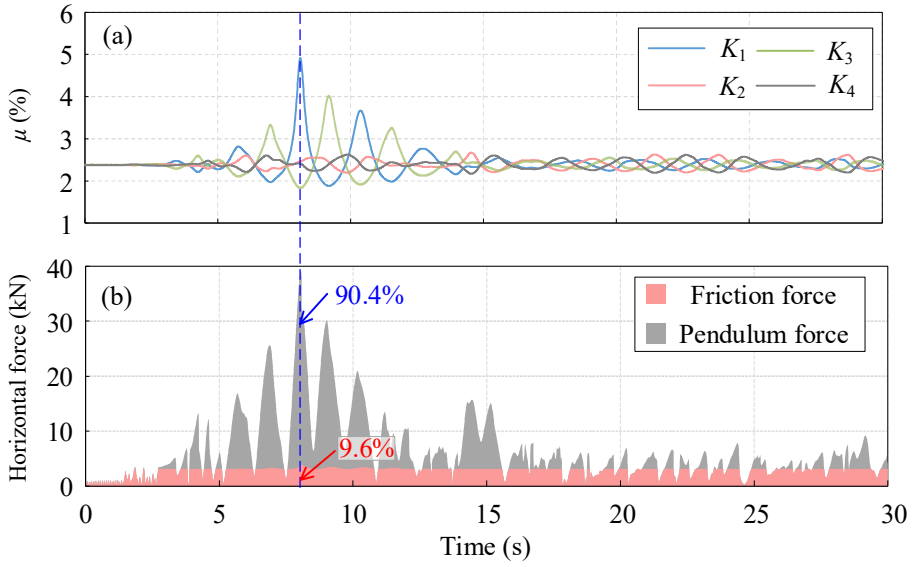

Fig. 20. Effect of the pressure-dependent friction coefficient: (a) variation in the friction coefficient, and (b) proportion of friction force.

On the other hand, the component tests in Section 3.2 also reveal bearing-to-bearing variability in the friction coefficient. To examine whether the additional torsion induced by this variability is consistent with that observed in the shake table tests, the initial friction coefficient of each full-scale FPB was randomly sampled while retaining the pressure-dependent friction model described above. A total of 100 sets of samples were generated, with the mean and standard deviation consistent with those obtained from the component tests. Time-history analyses were then performed using the corresponding randomly

This is the accepted version of the following article: Fu HR, Cao YT, Qu Z. Substructural shake table testing for nonstructural elements of various damage sensitivity in a fixed-base and a base-isolated building. ***Earthquake Engineering & Structural Dynamics***. This article may be used for non-commercial purposes.

sampled pressure-dependent friction coefficients in the finite element model. The log-normal distribution and the box plot of the numerical results under the maximum *PTA* condition, in comparison with the experimental data, are presented in Fig. 21.

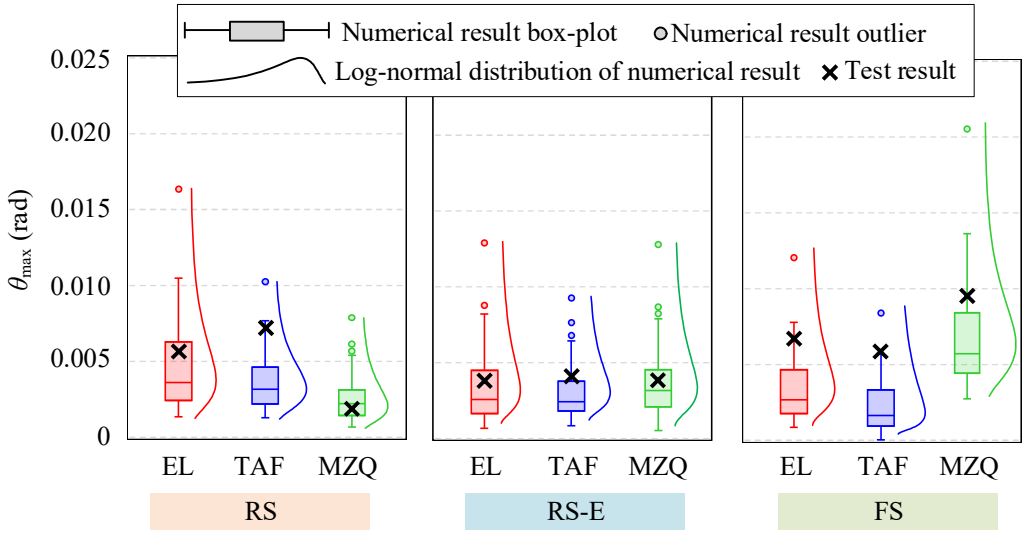

Fig. 21. Effect of friction-coefficient variability on θ_{max}.

The simulation results approximately follow a log-normal distribution, with the peak of the distribution skewed toward smaller values. Among the experimental results considered, four cases fall within the interquartile range of the box plots, indicating good agreement with the numerical simulations, while the remaining five cases fall within the whisker range and therefore remain within the reasonable bounds of the numerical results. Overall, these results suggest that, for nominally symmetric FPB-isolated structures, bearing-to-bearing variability in friction coefficients, arising from factors such as manufacturing tolerances or possible degradation, can be an important source of additional torsion. In contrast, both the pressure dependence of the friction coefficient and superstructure flexibility have relatively limited effects on the additional torsional response observed in the tests.

6 Conclusions

This study systematically investigates the torsional mechanism of FPB-isolated structures through analytical derivation, bearing component tests, full-scale shake table testing, and numerical simulation. The effective transient eccentricity (ε_s) is introduced to explain the influence of superstructure flexibility on the torsional response of FPB-isolated structures. The effects of the pressure dependence and bearing-to-bearing variability of the friction coefficient on the torsional response of the isolation layer are also examined. The main conclusions are as follows:

1. The effective transient eccentricity ε_s provides a more rational measure of the potential torsional behavior of FPB-isolated structures than the commonly used actual eccentricity ε_0 or transient eccentricity ε_k. Unlike ε_0, ε_k and λ, ε_s reflects not only the shift of the center of stiffness (CS) caused by the overturning moment, but also the positional relationship between the resultant base shear force and the CS, which directly governs the torsional response of the isolation layer.

2. In the FS system, the resultant base shear force V tends to deviate slightly from the CS of the isolation layer. As a result, ε_s exhibits noticeable fluctuations over the time domain, reaching a maximum of 4.45% when the *PTA* is 0.4 g in the numerical simulations. In contrast, in the RS and RS-E systems, ε_s remains much smaller for most of the response history.

This is the accepted version of the following article: Fu HR, Cao YT, Qu Z. Substructural shake table testing for nonstructural elements of various damage sensitivity in a fixed-base and a base-isolated building. ***Earthquake Engineering & Structural Dynamics***. This article may be used for non-commercial purposes.

3. The torsional responses observed in the tests result in only limited amplification of the maximum edge displacement. Under the maximum *PTA* conditions, all response-based values of λ are below 1.20, with a maximum value of only 1.041. In contrast, the torsional displacement amplification predicted by the conventional ASCE formulation is consistently larger than the response-based λ, indicating that this approach provides a relatively conservative estimate of torsional displacement amplification for FPB-isolated structures.

4. In the shake table tests, the measured torsional angles were noticeably larger than those predicted by the idealized numerical simulations. The results indicate that an important source of the additional torsional response is the inevitable scatter in the friction coefficients of FPBs within the same isolation layer, whereas the pressure dependence of the friction coefficient has only a marginal influence on the torsional behavior. This finding suggests that, for nominally symmetric FPB-isolated structures, variability in the properties of individual bearings associated with manufacturing tolerances and possible degradation may be a more critical source of unintended torsional response than mass eccentricity alone under the investigated conditions.

Acknowledgments

The study was funded by the Scientific Research Fund of Institute of Engineering Mechanics, China Earthquake Administration (2024C07, 2026B09).

Data Availability Statement

The data presented in this study are available on request from the corresponding author. The authors are willing to share the relevant data for research purposes.

References

Almazan, J. L., & de la Llera, J. C. (2003). Accidental torsion due to overturning in nominally symmetric structures isolated with the FPS. Earthquake Engineering & Structural Dynamics, 32(6), 919-948.

Becker, T. C., Keldrauk, E. S., Mieler, M. W., Mahin, S. A., & Stojadinovic, B. (2012, September). Effect of mass offset on the torsional response in friction pendulum isolated structures. 15th World Conference on Earthquake Engineering, Lisboa, Portugal.

Bertero, V. V., Mahin, S. A., & Axley, J. A. (1980, September). Lessons from structural damages observed in recent earthquakes. In Proceedings, 7th World Conference on Earthquake Engineering, Istanbul (Vol. 4, pp. 257-264).

Brown Jr, R. D., Ward, P. L., & Plafker, G. (1973). Geologic and seismologic aspects of the Managua. Nicaragua, earthquakes of December, 23, 1972.

Cao, Y., Fu, H., & Qu, Z. (2024). Experimental implementation of the nonstructural element simulator on shake table (NEST) for an archetype tall building. Earthquake Engineering & Structural Dynamics, 53(13), 3941-3962.

Cavdar, E., & Ozdemir, G. (2022). Amplification in maximum isolator displacement of an LRB isolated building due to mass eccentricity. Bulletin of Earthquake Engineering, 20(1), 607-631.

Constantinou, M. C., Tsopelas, P., Kasalanati, A., & Wolff, E. D. (1999). Property modification factors for seismic isolation bearings. Buffalo, NY: Multidisciplinary Center for Earthquake Engineering Research.

This is the accepted version of the following article: Fu HR, Cao YT, Qu Z. Substructural shake table testing for nonstructural elements of various damage sensitivity in a fixed-base and a base-isolated building. ***Earthquake Engineering & Structural Dynamics***. This article may be used for non-commercial purposes.

Chandler, A. M. (1986). Building damage in Mexico City earthquake. Nature, 320(6062), 497-501.

de la Llera, J. C., & Almazán, J. L. (2003). An experimental study of nominally symmetric and asymmetric structures isolated with the FPS. Earthquake Engineering & Structural Dynamics, 32(6), 891-918.

Fu, H., Cao, Y., & Qu, Z. (2024). Substructural shake table testing for nonstructural elements of various damage sensitivity in a fixed-base and a base-isolated building. Engineering Structures, 321, 119017.

Gokdemir, H., Ozbasaran, H., Unluoglu, E., & Albayrak, U. (2013). Effects of torsional irregularity to structures during earthquakes. Engineering Failure Analysis, 35, 713-717.

Jangid, R. S., & Datta, T. K. (1994a). Nonlinear response of torsionally coupled base isolated structure. Journal of Structural Engineering, 120(1), 1-22.

Jangid, R. S., & Datta, T. K. (1994b). Seismic response of torsionally coupled structure with elasto-plastic base isolation. Engineering Structures, 16(4), 256-262.

Hall, J. F., & Beck, J. L. (1986). Structural damage in Mexico city. Geophysical Research Letters, 13(6), 589-592.

Laguardia, R., Morrone, C., Faggella, M., & Gigliotti, R. (2019). A simplified method to predict torsional effects on asymmetric seismic isolated buildings under bi-directional earthquake components. Bulletin of Earthquake Engineering, 17(11), 6331-6356.

Lee, D. M. (1980). Base isolation for torsion reduction in asymmetric structures under earthquake loading. Earthquake Engineering & Structural Dynamics, 8(4), 349-359.

Mazza, F. (2017). Lateral-torsional response of base-isolated buildings with curved surface sliding system subjected to near-fault earthquakes. Mechanical Systems and Signal Processing, 92, 64-85.

McKenna, F. (2011). OpenSees: a framework for earthquake engineering simulation. Computing in Science & Engineering, 13(4), 58-66.

Meli, R., & Rosenblueth, E. (1986). The 1985 Earthquake causes and effects in Mexico City. Concrete International, ACI, Detroit, Mich, 8(5), 12.

Mokha, A. S., Amin, N., Constantinou, M. C., & Zayas, V. (1996). Seismic isolation retrofit of large historic building. Journal of Structural Engineering, 122(3), 298-308.

Nagarajaiah, S., Reinhorn, A. M., & Constantinou, M. C. (1993). Torsion in base-isolated structures with elastomeric isolation systems. Journal of Structural Engineering, 119(10), 2932-2951.

National Standards of the People's Republic of China. (2010). Code for seismic design of buildings (GB/T 50011-2010) [S]. Beijing: Standards Press of China. (in Chinese)

National Standards of the People's Republic of China. (2019). Friction pendulum isolation bearings for buildings (GB/T 37358-2019) [S]. Beijing: Standards Press of China. (in Chinese)

National Standards of the People's Republic of China. (2010). Technical specification for structures of tall building (JGJ 3-2010) [S]. Beijing: China Architecture & Building Press. (in Chinese)

National Standards of the People's Republic of China. (2015). Technical specification for steel structure of tall building (JGJ 99-2015) [S]. Beijing: China Architecture & Building Press. (in Chinese)

Olivares, C. I., de la Llera, J. C., & Poulos, A. (2020). Torsion control in structures isolated with the triple friction pendulum system. Engineering Structures, 216, 110503.

Ozer, E., Inel, M., & Cayci, B. T. (2022, March). Seismic behavior of LRB and FPS type isolators considering torsional effects. Structures. Elsevier, 2022, 37: 267-283.

Tsopelas, P., Constantinou, M. C., Kim, Y. S., & Okamoto, S. (1996). Experimental study of FPS system in bridge seismic isolation. Earthquake Engineering & Structural Dynamics, 25(1), 65-78.

This is the accepted version of the following article: Fu HR, Cao YT, Qu Z. Substructural shake table testing for nonstructural elements of various damage sensitivity in a fixed-base and a base-isolated building. ***Earthquake Engineering & Structural Dynamics***. This article may be used for non-commercial purposes.

544 Wolff, E. D., Ipek, C., Constantinou, M. C., & Morillas, L. (2014). Torsional response of seismically
545 isolated structures revisited. Engineering Structures, 59, 462-468.
546 Zayas, V. A., Low, S. S., & Mahin, S. A. (1990). A simple pendulum technique for achieving seismic
547 isolation. Earthquake Spectra, 6(2), 317-333.